Organic Electronics 15 (2014) 3327–3332

Contents lists available at ScienceDirect

Organic Electronics

journal homepage: www.elsevier.com/locate/orgel

High morphology stability and ambipolar transporting host for use in blue phosphorescent single-layer organic light-emitting diodes

Fang-Ming Hsu [a], Liang-Jung Chien [b], Kuan-Ting Chen [c], Ya-Ze Li [c], Shun-Wei Liu [c,*]

[a] Department of Applied Chemistry, National Chiao Tung University, Hsinchu 30010, Taiwan, Republic of China
[b] Department of Chemical Engineering, Ming Chi University of Technology, New Taipei City 24301, Taiwan, Republic of China
[c] Department of Electronic Engineering, Ming Chi University of Technology, New Taipei City 24301, Taiwan, Republic of China

ARTICLE INFO

Article history:
Received 1 June 2014
Received in revised form 14 August 2014
Accepted 6 September 2014
Available online 23 September 2014

Keywords:
Single layer
Phosphorescent materials
Organic light-emitting diode
Ambipolar host
Morphological stability
Recombination zone

ABSTRACT

The authors report a small molecule host of 2,7-bis(diphenylphosphoryl)-9-[4-(N, N-diphenylamino)phenyl]-9-phenylfluorene (POAPF) doped with 8 wt% iridium(III)-bis[(4,6-difluorophenyl)pyridinato-*N*,$C^{2'}$]picolinate (FIrpic) for use in efficient and single-layer blue phosphorescent organic light-emitting diodes (PHOLEDs) exhibiting a maximum external quantum efficiency of ~20.3% at brightness of 100 cd/m^2. The high performance of such single layer PHOLEDs is attributed to the POAPF host's high morphological stability, suitable triplet energy level, and equal charge carrier mobilities of hole and electron to form the broad carrier recombination zone in the emitting layer, thus reducing the triplet-triplet annihilation and resulting in a slight efficiency roll off of 0.5% from the brightness of 1 and 1000 cd/m^2. This work also systematically investigated the arrangement of the POAPF:FIrpic recombination zone for optimizing the performance of the single layer PHOLED.

1. Introduction

Highly efficient phosphorescent organic light-emitting diodes (PHOLEDs) have been successfully fabricated by solution process using large molecules (dendrimers and/or polymers) or by vacuum deposition of small electroluminescent (EL) molecules [1,2]. Based on these approaches, multilayer devices based on small molecules have been proposed to achieve high device performances through the selection of an appropriate material to tune the carrier transport and/or control the exciton distribution [3–5]. However, using such a multilayer structure with vacuum thermal deposition has several critical drawbacks, including complex device structures and high fabrication costs [6]. To the structure of such small-molecule devices can be simplified through the use of multiple-function materials in single-layer OLED applications.

Recently, many groups have demonstrated that the fluorescent or phosphorescent molecule can be used in vacuum processes for the fabrication of a single layer OLED with high performance [7–10]. For example, a boron-containing material has been proposed to demonstrate an efficient yellow-emitting single-layer device [11]. Lai et al. reported an ambipolar transporting host of benzimidazole/amine-based compounds in an orange/red-emitting phosphorescent single-layer device [12]. Using 3,7-bis[4-(N-carbazolyl)phenyl]benzo[1,2-b:4,5-b′] difuran as the host material, the resulting device exhibited well-balanced charge transport and high hole and electron mobilities of ~10^{-3} cm^2/V s, allowing for the fabrication of an efficient

* Corresponding author.
E-mail address: swliu@mail.mcut.edu.tw (S.-W. Liu).

http://dx.doi.org/10.1016/j.orgel.2014.09.009
1566-1199/

single layer device [13]. More recently, Wang et al. demonstrate that the emission properties of a top-emitting single-layer with p-i-n structure based on ambipolar host of 2,5-bis(2-(9H-carbazol-9-yl)phenyl)-1,3,4-oxadiazole are much higher than that for a multilayer device using the same emitting layer (EML) [14]. These results suggest that a host containing equal hole and electron mobilities and a high triplet energy level is required to improve the charge balance and exciton confinement in the single-layer PHOLED [15], especially in application for blue phosphorescent systems [16,17]. Based on the concept of exciton confinement in EML, our previous work demonstrated the use of a small molecule host containing triphenylamine and diphenylphosphorl-substituted fluorene units in the fabrication of highly efficient blue bilayer PHOLED because their high triplet gap (E_T of 2.75 eV) confines the triplet exciton in the emitting layer [18]. In addition, Yin et al. reported efficient white single-layer devices by co-doping blue and orange phosphorescent dyes to the 2,7-bis(diphenylphosphoryl)-9-[4-(N,N-diphenylamino)phenyl]-9-phenylfluorene (POAPF) [19]. Unfortunately, this approach did not systematically study the relationship between the material properties, i.e. carrier mobility and morphology stability, and single-layer device performance. Thus, this work uses electrical and EL characteristics, time-of-flight (TOF) measurement, and atomic-force microscopy (AFM) to address the effects of the POAPF:FIrpic recombination zone on single layer PHOLEDs.

2. Experiments

Organic materials 9,9-bis[4-(N,N-diphenylamino) pheny]fluorine (BPAF), POAPF, 3-(4-biphenylyl)-4-phenyl-5-(4-tert-butyl-phenyl)-1,2,4-triazole (TAZ), and phosphorescence dopant of iridium(III)-bis[(4,6-difluorophenyl)pyridinato-$N,C^{2'}$]picolinate (FIrpic) were synthesized by reported procedures [18], while blue dopant was purified twice in a home-made vacuum system according to the standard operation procedure in the literature [20]. The substrate was cleaned by ultrasonic bath in successive solutions of acetone and isoproponal, etched in a dilute solution of sulphuric acid, and finally dried by 5 N nitrogen blow. The single layer PHOLEDs were fabricated on a glass substrate coated with ITO anode (10 Ω/square). In addition, to improve the hole injection efficiency in our proposed device, a 35 nm PEDOT:PSS (CH8000; Clevios) was spin-coated on top of the ITO anode. To allow a performance comparison, various multilayer devices were also fabricated. The active area of our device was 4 mm^2 and all devices were encapsulated in a glove box. Fig. 1 shows the device configurations, energy levels, and chemical structures. The current density–voltage–luminance (J–V–L) characteristics of the OLED devices were measured using a dc current/voltage source meter (Keithley 2400), while the brightness was monitored with a spectrophotometer (Photo Research PR655). The AFM image of the organic thin films on a Si wafer was analyzed by a Park System XE-70 in

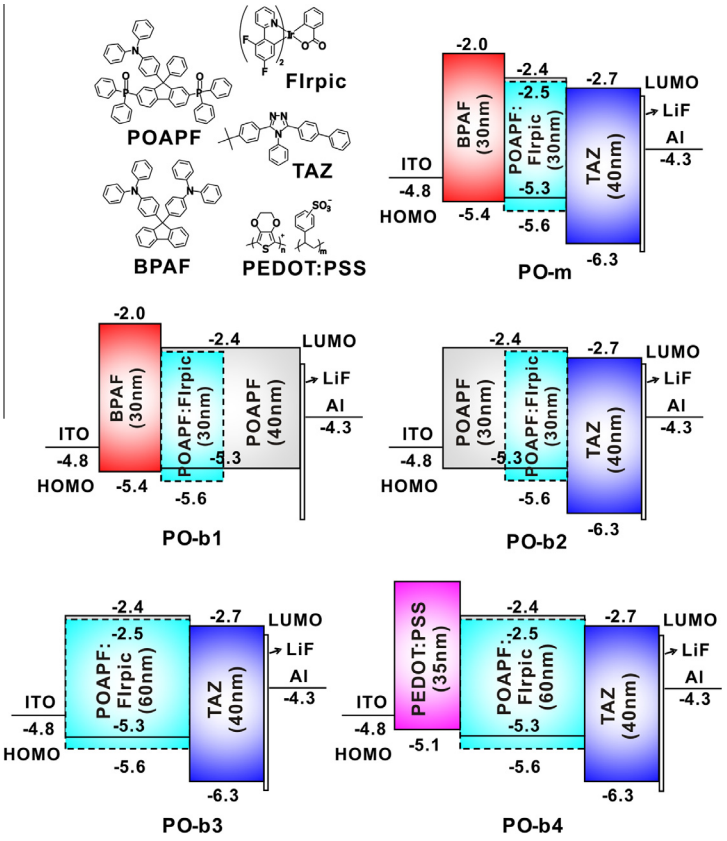

Fig. 1. Chemical structures, energy levels, and device configurations of PEDOT:PSS, BPAF, POAPF, TAZ, and FIrpic used in this study.

non-contact mode using a NCHR tip cantilever. The work-function of the ITO and the highest occupied molecular orbital (HOMO) level of the organic materials were measured using a photoelectron spectrometer (Riken Keiki AC-2). All measurements were carried out in an air environment.

For the TOF measurement, the POAPF ambipolar material was deposited at a constant rate of 0.3 nm/s on the ITO substrate to form a nearly 0.18–0.6 μm thick film, which was subsequently covered by 25 nm of Ag to form the electrode. The actual thickness of the organic layer was measured by a surface profiler (Dektak 150; Veeco). The frequency-doubled output of a 5 ns pulsed dye laser set at 295 nm was chosen to match the peak optical absorption of the organic layer. The laser was aimed at the samples from the semitransparent Ag electrode to generate carriers. The transient photocurrent created by the drift of the photoexcited carriers was monitored by a 2.5 GHz digital oscilloscope (LeCroy, WaveRunner 625Zi). To evaluate POAPF carrier mobility (μ), the hole or electron transient time was determined from the double-logarithmic plot of the TOF photocurrent versus the time characteristics and followed the Poole–Frenkel relationship to describe the increasing trend of field-dependent carrier mobility as the electric field strength increased. In addition, the μ was determined by $\mu = D/t_T E$, where D is the thickness of the organic layer, t_T is the transit time, and E is the applied electric field [21].

3. Results and discussion

Fig. 2 shows the J–V–L characteristics and external quantum efficiency (EQE) of various multilayer structures in POAPF based-devices. These devices include the previously reported highly efficient multilayered blue PHOLED (PO-m) with a configuration of ITO/BPAF (30 nm)/POAPF: 8 wt% FIrpic (30 nm)/TAZ (40 nm)/LiF (1 nm)/Al (100 nm) [18]. BPAF and TAZ were used as the hole-transporting layer (HTL) and the electron-transporting layer (ETL), respectively, because they have sufficiently high triplet energy gaps to confine the triplet excitons in the POAPF EML. Thus, the device **PO-m** exhibited the EQE and EL efficiencies reaching as high as 20.6% and 35.4 cd/A, respectively. To increase the efficiency of the blue PHOLED, we simplified the device architecture into a single-layer POAPF device, in an attempt to replicate the performance found in device **PO-m**. First, the POAPF layer was used as the electron- (PO-b1) or hole- (PO-b2) transporting layer in device **PO-m**. To provide a basis for comparing the effects of exciton-polaron annihilation and hole injection, we then used the bilayer structure of ITO/PEDOT:PSS (PO-b3: without and PO-b4: with) (35 nm)/POAPF: 8 wt% FIrpic (60 nm)/TAZ (40 nm)/LiF (1 nm)/Al (100 nm) to fabricate devices **PO-b1**, **PO-b2**, **PO-b3**, and **PO-b4**. As shown in Fig. 2, device **PO-b1** exhibited a high (EQE) of ~22.5% at 250 cd/m^2 because POAPF can be used as an electron-transporting and injecting layer in bilayer devices. This indicates that the POAPF can provide the effective material functions of carrier/exciton confinement, electron transporting, and electron injection in the ETL, thus improving the bilayer device performance. In contrast, device **PO-m** significantly outperformed devices **PO-b2** and **PO-b3** with the ITO/POAPF interface providing poor injection efficiency due to the large hole injection barriers. In addition, as compared to BPAF containing two-triphenylamine-segments, POAPF has only one triphenylamine segment in the molecule, which may degrade its hole-transporting ability. As mentioned above, we found that the current density or emission efficiency of device **PO-b3** is slightly higher than that of device **PO-b2** (see Fig. 2a). As noted by Lee et al., this is potentially because the high carrier mobility FIrpic doped into POAPF can generate a trap state suitable to improving the hole injection efficiency [22]. Recently, many groups have proposed inserting the PEDOT:PSS buffer between the ITO and HTL to improve hole injection and reduce exciton quenching near the electrode [23,24]. Thus, the performance of device **PO-b4** was similar to that of device **PO-m** because the PEDOT:PSS possesses a ladder-type (HOMO) level which facilitates hole-injection.

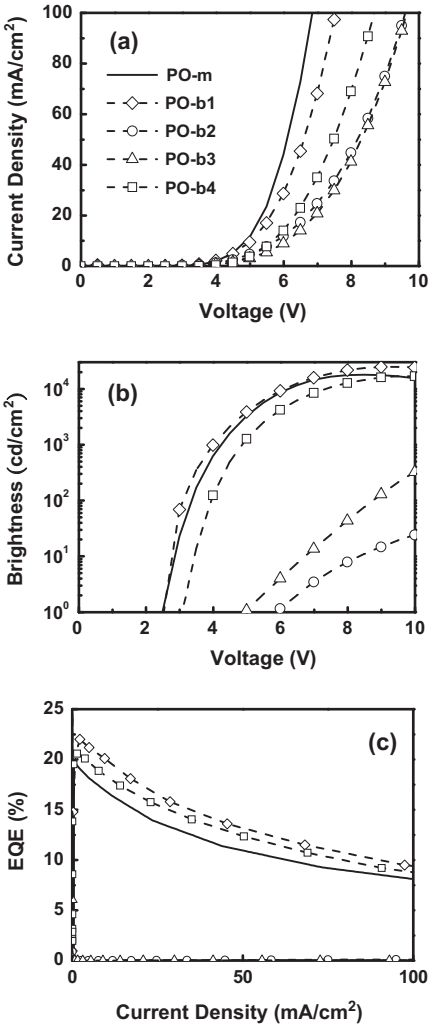

Fig. 2. (a) Current density *vs.* voltage, (b) brightness *vs.* voltage, and (c) external quantum efficiency *vs.* current density of various multilayer devices.

Another possible reason could be that the device's wide recombination zone significantly reduces the exciton quenching effect in PHOLED [25,26].

As shown in the inset of Fig. 3a, five devices were fabricated using the single-layer configuration to further confirm the recombination zone in the POAPF device. These devices were fabricated using the following configuration: ITO/PEDOT:PSS (35 nm)/POAPF (PO-0:x = 0, PO-20:x = 20, PO-40:x = 40, PO-60:x = 60, and PO-80:x = 80 nm)/POAPF:8 wt% FIrpic (20 nm)/POAPF(80−x nm)/LiF (1 nm)/Al (100 nm). The total thickness of the single-layer device was under 100 nm. On the other hand, to evaluate the charge balance in the single-layer POAPF device, we also fabricated device **PO-s** with a 100 nm emitting layer, i.e., ITO/PEDOT:PSS/POAPF:8 wt%FIrpic/LiF/Al. As shown in Fig. 3a, the electrical characteristics of all single-layer devices (PO-x series) were almost identical indicating that altering the HTL or ETL thickness does not induce the extra trap or alter the carrier transporting properties of single-layer POAPF devices. Despite the similar electrical characteristics of these single-layer devices, their EL spectra and emission efficiency are quite different from that found in the single-layer devices (see Fig. 3b and c). For example, the devices **PO-60** and **PO-80** exhibited relatively poor emission efficiency due to charge imbalance as well as the formation of an emission zone near the ITO/POAPF which induced additional exciton quenching. More interestingly, the emission profile of device **PO-80** (see Fig. 3d) with high electric field is similar to that of device **PO-0** (see Fig. 3b). This result suggests that high performance is dependent on controlling the recombination zone in single-layer POAPF.

Devices **PO-0** and **PO-20** exhibited a pure FIrpic emission spectrum because the recombination zone is completely confined in the EML. Using this confinement strategy in a single-layer device, device **PO-s** with a wide EML showed high EQE values 20.3% than devices **PO-m**, **mCP-s**, and **mCP-m**. Note that the architectures of devices **mCP-s** and **mCP-m** were respectively identical to **PO-s** and **PO-m**, and both devices used the conventional host material N,N′-dicarbazolyl-3,5-benzene (mCP). For comparison, Table 1 summarizes the EL data (driving voltage, EQE, power efficiency, current efficiency, and Commission Internatonale de L'éclairage coordinate) of all devices. In the measured results, the EL performance of device **PO-s** (EQE ~20.3%) is comparable with that of device **PO-m** (EQE ~20.6%), both of which significantly outperform devices **mCP-s** and **mCP-m** (EQE ~13%). However, we observed that the performance of device **PO-s** is slightly lower than that of device **PO-b1** because the single-layer device can not completely confine the recombination zone in central region to avoid exciton quenching. Note that the performance of PO-s is still much higher than that of single-layer green PHOLED based on high carrier mobility and ambipolar transporting 4,4′-N,N′-dicarbazolylbiphenyl host (EQE ~13.3%) [9,27].

We attribute this improved performance of device **PO-s** to the POAPF host's ambipolar transporting ability and good thermal or morphological stability to form the broad carrier recombination zone in single-layer PHOLEDs, resulting in the alleviation of undesired exciton quenching [28]. Fig. 4 shows the TOF result to confirm our hypothesis regarding the transporting property (hole or electron) of POAPF. The POAPF host clearly exhibits rare ambipolar charge transport properties with mobility in the order of $\sim 10^{-6}$ cm^2/V s. However, this result was very consistent with our design rule for the synthesis of POAPF [18]. More recently, several studies have successfully used the

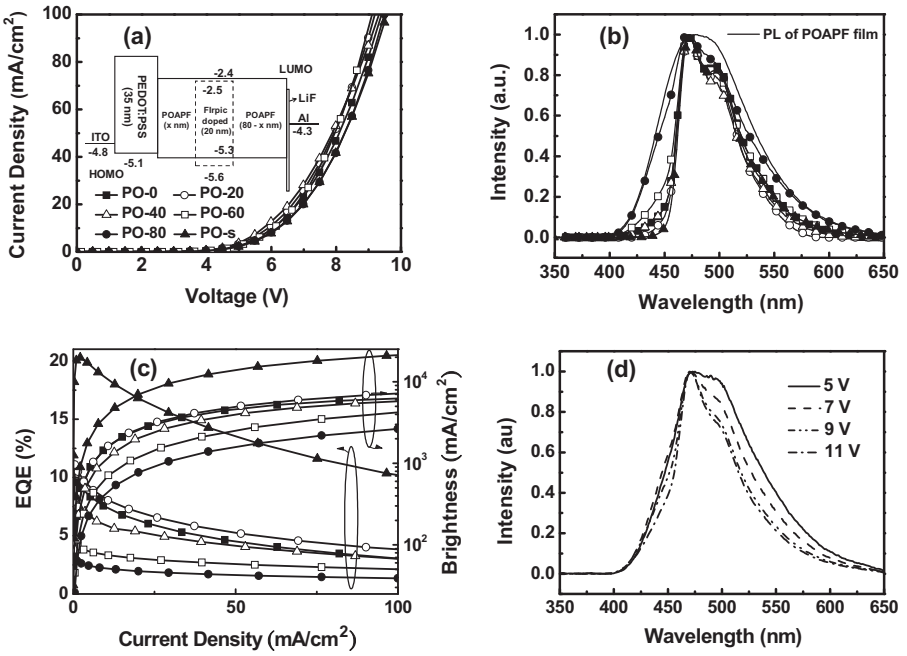

Fig. 3. (a) Current density *vs.* voltage, (b) EL spectra, and (c) external quantum efficiency *vs.* current density of various single-layer devices. (d) The EL spectra of device PO-80 under different applied voltage. Note that the inset figure shows the device configuration of single-layer POAPF devices.

Table 1
Electroluminescence data for the devices.

Device	PO-m	PO-b1	PO-b2[d]	PO-b3[d]	PO-b4	PO-0	PO-20	PO-40	PO-60	PO-80	PO-s	mCP-s[d]	mCP-m
V[a] (V)	2.5/4.2	2.5/4.0	6.0/–	5.0/–	3.0/4.8	3.0/5.6	3.0/5.4	3.0/5.6	3.0/6.4	3.0/7.4	3.0/5.0	10.8/–	3.8/6.6
EQE[b] (%)	20.6/18.8	22.0/21.8	–/–	–/–	20.8/20.2	9.6/8.2	11.1/9.0	7.8/6.1	4.6/3.2	3.3/1.8	20.3/20.2	–/–	13.2/11.2
PE[b] (lm/W)	36.7/24.3	35.2/35.1	–/–	–/–	24.7/22.8	15.6/9.5	16.5/9.8	11.8/6.5	8.2/3.1	5.9/1.6	26.5/26.2	–/–	14.9/9.6
LE[b] (cd/A)	35.4/32.3	44.8/44.7	–/–	–/–	35.8/34.8	19.8/16.9	21.0/17.0	15.0/11.7	9.1/6.2	6.6/3.6	42.2/42.1	–/–	23.7/20.1
CIE[c] (x, y)	0.13,0.27	0.14,0.34	0.14,0.34	0.14,0.34	0.11,0.28	0.15, 0.33	0.12,0.31	0.14, 0.31	0.16,0.30	0.18,0.28	0.15,0.35	–	0.12,0.29

[a] Measured operating voltages, presented in the order of the values at 1 and 1000 cd/m^2.
[b] Measured values, presented in the order of the maximum value and the value at 1000 cd/m^2.
[c] Measured at 7 V.
[d] The devices showed the very poor electroluminescence property. (PO-b2:11 cd/m^2 at a driving voltage of 8.5 V; PO-b3:14 cd/m^2 at a driving voltage of 7.0 V; mCP-s:12 cd/m^2 at a driving voltage of 12 V.)

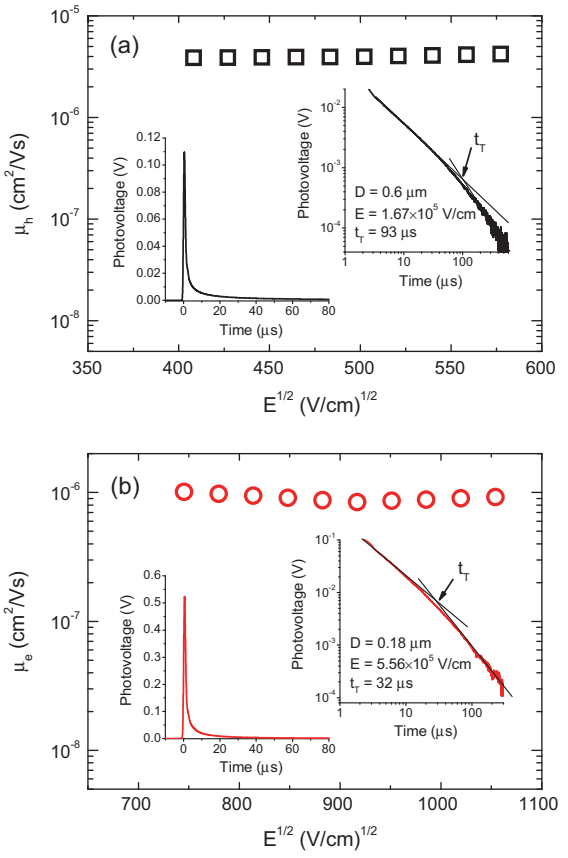

Fig. 4. (a) Hole and (b) electron mobilities plotted with respect to square root of applied electric field. Insets: double-linear and double-logarithmic plots of TOF transient profiles.

concept of balancing the holes and electrons in the EML to improve the performance of single-layer devices [29,30,10]. In addition, the TOF transient photocurrents for POAPF holes and electrons (insets to Fig. 4a and b) exhibited highly dispersive profiles due to the presence of a large local site-energy in the host which induced the board charge carrier distributions [31]. This phenomenon is in agreement with previous assumption that the single-layer POAPF device features a broad carrier recombination zone. In order to further study the issue of the EML property, we expect that the good thermal stability of POAPF can provide stable injection and transporting properties in the EML, which suggests the lifetime of the POAPF-based device is longer than that of its mCP-based counterpart. Thus, it is well known that the carrier mobility of an organic semiconducting layer can be effectively improved by using a thermal annealing [32,33]. Therefore, we observed that the thermal effect improves the carrier mobility of POAPF thin film to form a good molecule-packing configuration and induce a smoother morphology in POAPF, resulting in increased carrier mobility in the POAPF host as shown in Fig. 5. Although the POAPF exhibits a good thermal stability and ambipolar transporting property, the hole or electron carrier mobility of POAPF is still lower than that of common HTL or ETL [34,35]. Thus it is reasonably explained that we have observed that device **PO-s** or **PO-x** showed high driving voltage as compared with device **PO-m**.

Fig. 6 shows the AFM images of POAPF and mCP hosts with thermal annealing at ~100 °C for 12 h. The surface profile of the root mean square (rms) image is measured to be 0.38 nm for POAPF. Most importantly, the POAPF thin film exhibits a very smooth and stable surface morphology as compared with the mCP host (see Fig. 6). In fact, the formation of a highly smooth host is a key factor in

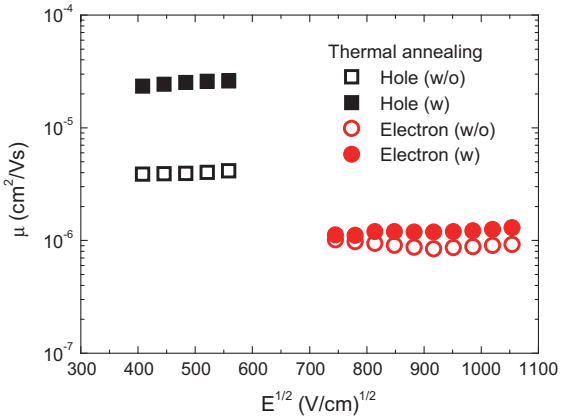

Fig. 5. Carrier mobilities plotted with respect to $E^{1/2}$ without (w/o) and with (w) thermal annealing.

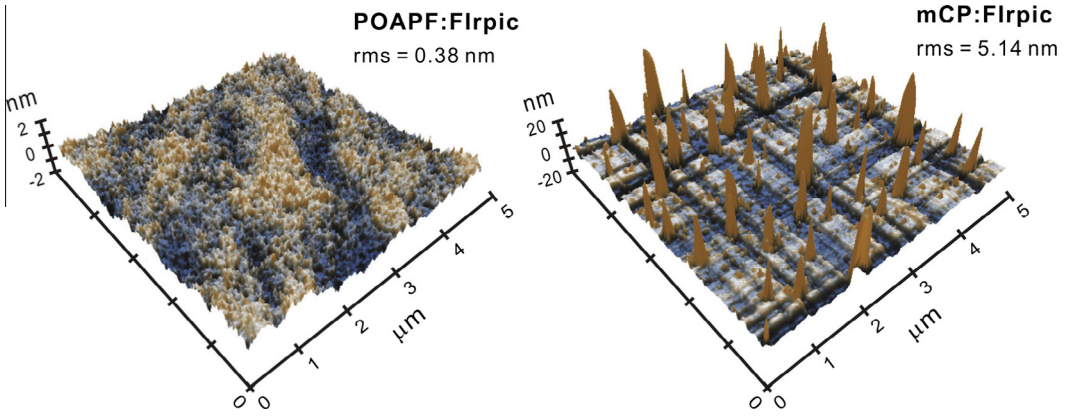

Fig. 6. AFM images of POAPF and mCP hosts doped with 8% FIrpic with thermal annealing.

determining the injection efficiency at the anode/organic or cathode/organic interface. Our experiment results demonstrate that the single-layer device **PO-s** has potential to serve as an alternative to the traditional multilayer architecture in PHOLEDs.

4. Conclusion

We have demonstrated a highly efficient single-layer blue PHOLED based on the POAPF host doped with 8 wt% FIrpic fabricated via a step-by-step method to simplify the conventional multilayer structures. The single-layer **PO-s** device with an EQE of ~20.3% exhibited EL performance similar to that of the multilayer **PO-m** device. In addition, the ambipolar transporting ability and stable morphology properties of the POAPF may significantly improve the charge balance and reduce undesired exciton quenching, thus significantly improving the performance of single-layer devices.

Acknowledgments

The authors acknowledge the financial support from the National Science Council (Grant Nos. NSC 102-3113-E-001-001, NSC 102-2627-E-002-002, NSC 102-2221-E-011-142, NSC 102-2511-S-131-002, NSC 102-2221-E-131-030-MY2, NSC 102-2221-E-131-026-MY2, MOST 103-2627-E-002-002, and MOST 103-2622-E-131-007-CC3). In addition, the author (Dr. F.M. Hsu) would like to give special thanks to Prof. Ching-Fong Shu (NCTU) for supplied the POAPF materials in this work.

References

[1] C. Adachi, M.A. Baldo, M.E. Thompson, S.R. Forrest, J. Appl. Phys. 90 (2001) 5048.
[2] S.-J. Su, D. Tanaka, Y.-J. Li, H. Sasabe, T. Takeda, J. Kido, Org. Lett. 10 (2008) 941–944.
[3] H. Sasabe, K. Minamoto, Y.-J. Pu, M. Hirasawa, J. Kido, Org. Electron. 13 (2012) 2615–2619.
[4] S.E. Jang, K.S. Yook, J.Y. Lee, Org. Electron. 11 (2010) 1154–1157.
[5] N. Chopra, J.S. Swensen, E. Polikarpov, L. Cosimbescu, F. So, A.B. Padmaperuma, Appl. Phys. Lett. 97 (2010) 033304.
[6] H.B. Wu, J.H. Zou, F. Liu, L. Wang, A. Mikhailovsky, G.C. Bazan, W. Yang, Y. Cao, Adv. Mater. 20 (2008) 696–702.
[7] H.-H. Chang, W.-S. Tsai, C.-P. Chang, N-P. Chen, K.-T. Wong, W.-Y. Hung, S.-W. Chen, Org. Electron. 12 (2011) 2025–2032.
[8] S.-W. Liu, Y.-T. Chang, C -C. Lee, C.-H. Yuan, L.-A. Liu, Y.-S. Chen, C.-F. Lin, C.-I. Wu, C.-T. Chen, Jpn. J. Appl. Phys. Lett. 52 (2013) 012101.
[9] Z.M. Hudson, Z. Wang, M.G. Helander, Z.H. Lu, S. Wang, Adv. Mater. 24 (2012) 2922–2928.
[10] Y. Liu, L.-S. Cui, M.-F. Xu, X.-B. Shi, D.-Y. Zhou, Z.-K. Wang, Z.-Q. Jiang, L.S. Liao, J. Mater. Chem. C 2 (2014) 2488–2495.
[11] H. Zhang, C. Huo, J. Zhang, P. Zhang, W. Tian, Y. Wang, Chem. Commun. (2006) 281–283.
[12] M.-Y. Lai, C.-H. Chen, W.-S. Huang, J.-T. Lin, T.-H. Ke, L.-Y. Chen, M.-H. Tsai, C.-C. Wu, Angew. Chem. Int. Ed. 47 (2008) 581–585.
[13] H. Tsuji, C. Mitsui, Y. Sato, E. Nakamura, Adv. Mater. 21 (2009) 3776–3779.
[14] Q. Wang, Y. Tao, X. Qiao, J. Chen, D. Ma, C. Yang, J. Qin, Adv. Funct. Mater. 21 (2011) 1681–1686.
[15] J. Huang, G. Li, E. Wu, Q. Xu, Y. Yang, Adv. Mater. 18 (2006) 114–117.
[16] W.-Y. Hung, Z.-W. Chen, H.-W. You, F.-C. Fan, H.-F. Chen, K.-T. Wong, Org. Electron. 12 (2011) 575–581.
[17] Y. Chen, J. Chen, Y. Zhao, D. Ma, Appl. Phys. Lett. 100 (2012) 213301.
[18] F.-M. Hsu, C.-H. Chien, C.-F. Shu, C.-H. Lai, C.-C. Hsieh, K.-W. Wang, P.-T. Chou, Adv. Func. Mater. 19 (2009) 2834–2843.
[19] Y. Yin, X. Piao, Y. Li, Y. Wang, J. Liu, K. Xu, W. Xie, Appl. Phys. Lett. 101 (2012) 063306.
[20] C.-C. Chi, C.-L. Chiang, S.-W. Liu, H. Yueh, C.-T. Chen, C.-T. Chen, J. Mater. Chem. 19 (2009) 5561–5571.
[21] C.-H. Hsiao, S.-W. Liu, C.-T. Chen, J.-H. Lee, Org. Electron. 11 (2010) 1500–1506.
[22] Y. Li, K. Xu, X. Wen, L. Zhang, Y. Yin, S. Liu, X. Piao, W. Xie, Org. Electron. 14 (2013) 1946–1951.
[23] P.A. Lane, G.P. Kushto, Z.H. Kafafi, Appl. Phys. Lett. 90 (2007) 023511.
[24] M.A. Baldo, R.J. Holmes, S.R. Forrest, Phys. Rev. B 66 (2002) 035321.
[25] C. Adachi, M.A. Baldo, S.R. Forrest, M.E. Thompson, Appl. Phys. Lett. 77 (2000) 904–906.
[26] N.C. Erickson, R.J. Holmes, Adv. Funct. Mater. 23 (2013) 5190–5198.
[27] J.-W. Kang, S.-H. Lee, H.-D. Park, W.-I. Jeong, K.-M. Yoo, Y.-S. Park, J.-J. Kim, Appl. Phys. Lett. 90 (2007) 223508.
[28] F.-M. Hsu, C.-H. Chien, Y.-J. Hsieh, C.-H. Wu, C.-F. Shu, S.-W. Liu, C.-T. Chen, J. Mater. Chem. 19 (2009) 8002–8008.
[29] C.-C. Lee, C.-H. Yuan, S.-W. Liu, L.-A. Liu, Y.-S. Chen, J. Display Technol. 7 (2011) 636–639.
[30] S.-W. Liu, C.-H. Yuan, S.-J. Yeh, M.-F. Wu, C.-T. Chen, C.-C. Lee, J. Soc. Inf. Display 19 (2011) 346.
[31] Y. Shirota, H. Kageyama, Chem. Rev. 107 (2007) 953–1010.
[32] B.J. Chen, X.W. Sun, T.K.S. Wong, X. Hu, A. Uddin, Appl. Phys. Lett. 87 (2005) 063505.
[33] C.Y. Kwong, A.B. Djurišić, V.A.L. Roy, P.T. Lai, W.K. Chan, Thin Solid Films 458 (2004) 281–286.
[34] K.R. Justin Thomas, M. Velusamy, J.T. Lin, C.H. Chien, Y.-T. Tao, Y.S. Wen, Y.-H. Hu, P.-T. Chou, Inorg. Chem. 44 (2005) 5677–5685.
[35] H.-F. Chen, S.-J. Yang, Z.-H. Tsai, W.-Y. Hung, T.-C. Wang, K.-T. Wong, J. Mater. Chem. 19 (2009) 8112–8118.